University of Birjand

Water Harvesting Research (2026) Vol. 9, No. 1: 28-39

10.22077/jwhr.2026.10498.1191

ORIGINAL ARTICLE

Water Extent Monitoring Using Sentinel-2 (Case Study: Latyan Dam Reservoir)

Amirhossein Maeli[a], Amirali Alavi [a], Ehsan Vasheghani Farahani[a*], Mahmoud Mashal[a], Armin Nasrollahi[a]

[a]Department of Water Engineering, Faculty of Agricultural Technology, College of Agriculture and Natural Resources, University of Tehran, Tehran, Iran.

[*]Corresponding Author E-mail Address: ehsan.farahani@ut.ac.ir

Received: 16 November 2025, **Revised**: 20 February 2026, **Accepted**: 09 March 2026

Abstract

Monitoring the surface area of reservoirs is crucial for effective water resource management, particularly in arid and semi-arid regions where water availability fluctuates significantly. This study utilizes Sentinel-2 imagery to assess water extent variations in the Latyan Dam reservoir in Iran from 2016 to 2024. By applying three well-established water indices—NDWI, MNDWI, & AWEIsh—water surface areas were delineated. Sentinel-2 Level-2A images, preprocessed using the Sen2Cor algorithm, were analyzed in SNAP software, ensuring high accuracy in atmospheric correction and reflectance values. The derived water area was validated using index intersection and union approaches to refine detection accuracy. The reservoir's surface area showed a clear declining trend, decreasing from 3.3 km² in 2016 (wettest year) to 1.1 km² in 2023 (driest year), corresponding to a shrinkage of about 2.2 km². Throughout 2016–2024, the uncertainty band between the union and intersection of NDWI, MNDWI, and AWEIsh remained relatively narrow, fluctuating between approximately 0.2 and 0.4 km², with slightly lower values in drier years. Applying Otsu thresholding substantially increased the number of uncertain water pixels compared to the fixed global threshold (index ≥ 0), from 3446 to 8250 pixels in 2016 and from 1718 to 7191 pixels in 2023, indicating that the global threshold provides more stable and conservative water detection for long-term monitoring. This approach provides an efficient, replicable methodology for large-scale water monitoring, supporting sustainable water resource management and policy decisions.

Keywords: Dam Monitoring, Drought Monitoring, NDWI, Remote Sensing, Satellite Imagery, Water Area.

1. Introduction

Monitoring the surface area of water bodies, particularly in reservoirs, is a crucial aspect of water resource management. This is especially important in arid and semi-arid regions, where water availability is highly variable and often scarce. In such regions, the extent of water surface at the end of a water year serves as an indicator of the overall status of water resources (Assiri et al. 2024). It reflects the balance between water recharge and consumption, offering insights into hydrological processes such as rainfall variability, evapotranspiration rates, and supply–demand dynamics (Gu et al. 2021).

Traditional methods for monitoring water surface area include in-situ measurements and aerial surveys. Although these approaches provide accurate and detailed data, they are often labor-intensive, costly, and limited in spatial and temporal coverage. Advances in remote sensing technologies have introduced more efficient alternatives based on satellite imagery, which offer broader spatial coverage and higher temporal frequency, making them suitable for large-scale monitoring (Alahacoon and Edirisinghe 2022). However, earlier remote sensing platforms were sometimes constrained by low spatial resolution or high operational costs, limiting their applicability.

Recent studies have increasingly relied on multispectral satellite imagery and spectral water indices to improve the accuracy of water surface delineation. Ozelkan (2019) evaluated three NDWI-based models—NDWI (Green, NIR), NDWI (Green, SWIR1), and NDWI (Green, SWIR2)—using Landsat imagery with 15 m and 30 m spatial resolutions to detect the surface water area of Atikhisar Dam Lake. The results indicated that NDWI(Green, NIR) achieved the highest accuracy, with RMSE values of 0.068 km² (15 m) and 0.076 km² (30 m), while the other indices showed greater sensitivity to land cover changes.

Similarly, Ticehurst et al. (2022) assessed surface water extent in the Murray–Darling Basin by combining multiple indices, including MNDWI, FWI, WOfS, and TCW, derived from Landsat imagery. Their findings demonstrated that although individual indices performed adequately, combining them in their optimal environmental contexts increased water pixel detection accuracy to between 90.5% and 94.8%.

Rokni et al. (2014) investigated water extent changes in Lake Urmia using several spectral indices such as NDWI, MNDWI, NDMI, WRI, NDVI, and AWEI. Their analysis showed that NDWI achieved the highest classification accuracy (99.88%), followed closely by NDVI (99.71%). A subsequent application of a Principal Component approach slightly reduced accuracy (99.86%), confirming the robustness of the NDWI method.

Other studies have applied spectral indices under varying climatic and environmental conditions. Mizuochi et al. (2014) analyzed water distribution in north-central Namibia using MODIS and AMSR datasets, applying NDWI and NDPI indices. Their results demonstrated moderate classification performance, highlighting the influence of sensor characteristics and environmental conditions on water detection accuracy. Koto et al. (2026) employed the AWEIsh index with Landsat imagery for surface water detection, emphasizing its ability to reduce shadow-related misclassification and its straightforward discrimination between water (positive values) and non-water (negative values). Likewise, Melkamu et al. (2022) evaluated NDWI, MNDWI, AWEIsh, and AWEInsh for monitoring Lake Beseka in Ethiopia and confirmed the effectiveness of spectral indices in distinguishing water from surrounding land cover types.

Among current satellite platforms, Sentinel-2 imagery has emerged as a particularly valuable tool due to its high spatial resolution, multispectral capability, and free accessibility. These characteristics enable more precise delineation of water bodies, even under challenging conditions such as turbidity variations or adjacent vegetation (Varghese et al. 2021). Despite the extensive application of water indices in different regions, further case-specific evaluations remain essential, particularly in reservoirs located in arid and semi-arid environments where hydrological variability is significant.

The purpose of this study is to demonstrate a systematic method for deriving reservoir water surface area using Sentinel-2 imagery and established indices, including NDWI, MNDWI, and AWEIsh. By applying this framework to the Latyan Dam Reservoir, this study aims to provide a reliable, reproducible, and efficient approach for water surface monitoring. SNAP software was utilized for image processing and water area extraction, and the procedure is described step-by-step to facilitate application in other study areas. The findings contribute to improved water resource assessment and support decision-making processes in water-scarce regions.

2. Materials and Methods

2.1. Study Area

This study focuses on the Latyan Dam, a vital infrastructure providing 30% of Tehran's drinking water. Located at 35.790°N latitude and 51.678°E longitude, this concrete dam plays a critical role in the region's water management (Fig. 1). With a catchment area of 702 square kilometers, the dam annually supplies approximately 290 million cubic meters of drinking water and 160 million cubic meters of agricultural water. Additionally, about 140 million cubic meters are transferred annually from the Lar Dam to the Latyan Dam's reservoir to meet Tehran's water demands. These activities collectively support the region's agricultural, urban, and energy needs, including the generation of 700,000

megawatt-hours of hydroelectric power for the national grid.

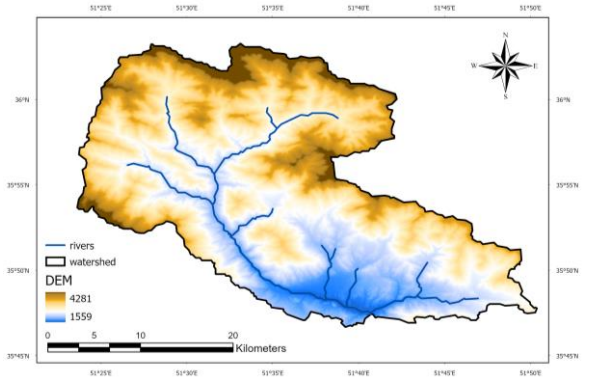

Fig. 1. Location of Latyan dam basin

The watershed surrounding the Latyan Dam is predominantly semi-arid, covering 572 square kilometers as of 2020. Land cover changes, influenced by urbanization and agricultural development, have significantly impacted the hydrology and water quality of the area. Increased impervious surfaces reduce groundwater recharge and base flows, while deforestation and agricultural expansion contribute to higher sediment loads and water pollution. The region experiences an average annual precipitation of 234 mm, with an estimated evapotranspiration of 171 mm per year. These estimates are derived from global datasets such as WorldClim and GLEAM, which provide insights into the watershed's climatic and hydrological dynamics. The Latyan Dam, with a total storage capacity of 95 million cubic meters, exemplifies the challenges and opportunities in managing water resources in arid and semi-arid regions.

2.2. Satellite Selection (Sentinel-2 Multi-spectral Imager)

Large-scale water body extraction has been explored using various indices with satellites like MODIS (Sharma et al. 2015) and Landsat (Wang et al. 2018). However, recent advancements in high-resolution remote sensing technologies, such as Sentinel-2, offer significant improvements. Alternatives like Gaofen-2 Satellite (GF-2) and SPOT-5, 6, and 7 provide high spatial resolution (1–4 m and 1.5–10 m, respectively) but lack SWIR bands essential for water body detection using indices (Liu et al. 2022). Sentinel-2 provides a spatial resolution of 10–60 meters, a five-day revisit cycle, and 13 spectral bands, making it ideal for water-related studies (Drusch et al. 2012).

2.3. Data Collection

Images of the study area from 2016 to 2024 were downloaded from the Copernicus Open Access Hub. Level-2A images were used due to their surface reflectance correction via the Sen2Cor algorithm, which removes atmospheric effects like aerosols and water vapor. In contrast, Level-1C images require additional computational resources for correction. This preprocessing ensures higher accuracy for applications such as land cover classification and environmental monitoring.

2.4.Water Indices Calculation

Sentinel-2 imagery provides 13 spectral bands with varying resolutions. For water area analysis (calculation of three indices), only VIS bands, NIR (B8), and SWIR (B11, B12) bands were used. The indices (NDWI, MNDWI and AWEIsh) applied are as equations of Table 1:

Table 1. Implemented water indices and their equations

Index	Formula	
NDWI (Normalized Difference Water Index)	$NDWI = \frac{Green(B3) - NIR(B8)}{Green(B3) + NIR(B8)}$	(1)
MNDWI (Modified Normalized Difference Water Index)	$MNDWI = \frac{Green(B3) - SWIR(B11)}{Green(B3) + SWIR(B11)}$	(2)
AWEIsh (Automated Water Extraction Index shadow)	$AWEIsh = \begin{pmatrix} Blue(B2) + 2.5Green(B3) \\ -1.5\ x\ (NIR(B8) + SWIR1(B11)) \\ -0.25\ x\ SWIR2(B12) \end{pmatrix}$	(3)

2.4.1. NDWI

NDWI exploits water's high reflectance in the green band and low reflectance in NIR, yielding values between -1 and 1. Values close to 1 indicate water presence, while values near 0 or negative signify vegetation or soil. However, NDWI may overestimate water areas in dense vegetation or shadowed regions and is sensitive to polluted waters (McFeeters, 1996) (Du et al. 2016).

2.4.2. MNDWI

Replacing the NIR band with SWIR improves NDWI performance by reducing errors from built-up areas due to SWIR's higher reflectance for buildings. Positive values near 1 indicate water, while values near 0 or negative correspond to vegetation or urban areas (Chen et al. 2015).

2.4.3. AWEIsh

Designed to address inaccuracies in other indices, AWEIsh is effective in shadowed areas by eliminating noise from ground objects with similar water-like properties (Feyisa et al. 2014).

2.5. Data Analysis Methods

Analysis was performed on Level-2 images using SNAP software through the following steps:

1. **Resampling:** SWIR band resolution (20m) was resampled to 10 m using bilinear interpolation to match other bands (Du et al. 2016; Liu et al. 2022).
2. **Subsetting:** The region of interest was extracted to reduce computational effort and focus on relevant areas.
3. **Band Math and Graph Processing:** Indices were calculated using band math, and a Graph Processing Tool (GPT) automated these calculations for multiple images. The results were further refined using two approaches:
   - Intersection: Areas identified as water by all indices (lower band, Eq. 4).
   - Union: Areas identified as water by at least one index (upper band, Eq. 5).

$$If\ (NDWI \geq 0\ \&MNDWI \geq 0\ \&\ AWEIsh \geq 0)\ Then\ 1\ else\ 0 \quad (4)$$

$$If\ (NDWI \geq 0\ or\ MNDWI \geq 0\ or\ AWEIsh \geq 0)\ Then\ 1\ else\ 0 \quad (5)$$

4. **Water Area Mask Creation:** A binary mask was generated for water areas based on index thresholds.
5. **Visualization:** Results were visualized using ArcGIS Pro for easier interpretation.

Graphs in Fig. 2a and 2b were both utilized for the analysis where the graph in Fig. 2a was applied for the processing of the collected images by resampling and subsetting them and the graph in Fig. 2b was used to compute the water indices. Also, in Fig. 2b, Band math 1 to 3 correspond to the indices NDWI, MNDWI, and AWEIsh, respectively.

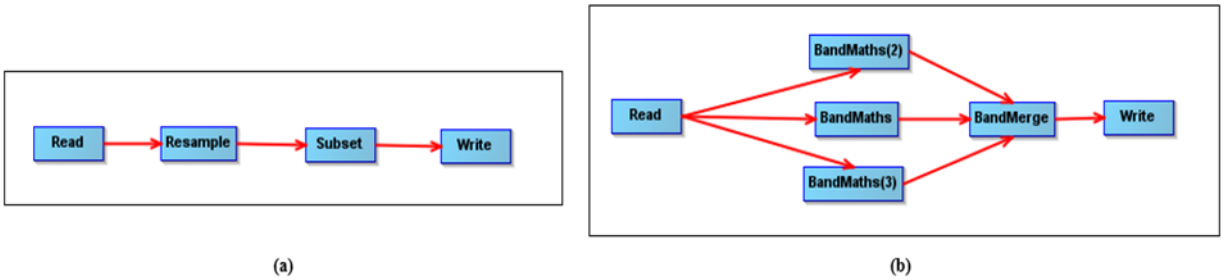

Fig. 2. Graphs used for a: Processing the images, b: Computation the water indices

2.6. Otsu Thresholding

Otsu algorithm is a non-parametric thresholding method based on image's gray histogram. This method separates the image into 2 segments of Foreground (Water) & Background (Non-water) in appropriate to the optimal value. The optimal value is considered to be the one that it maximizes the interclass variance & minimizes the intraclass variance (Tang et al. 2022).

3. Results and Discussion

The image processing resulted in yearly maps for three remote sensing indices (NDWI, MNDWI, and AWEIsh), as well as the lower and upper bands derived from their intersection and union. Figure 3a, which is the

result for 2016, illustrates the lower band (highlighted in blue) and the upper band (red boundary), which represent the water areas determined by the union and intersection of the indices. These bands were used to assess the water body extents across the study period. In Fig. 3b, the difference between the upper and lower bands, calculated as (Union - Intersection) using ArcGIS Pro, is displayed. This difference highlights the variability and uncertainty in water body detection among the indices.

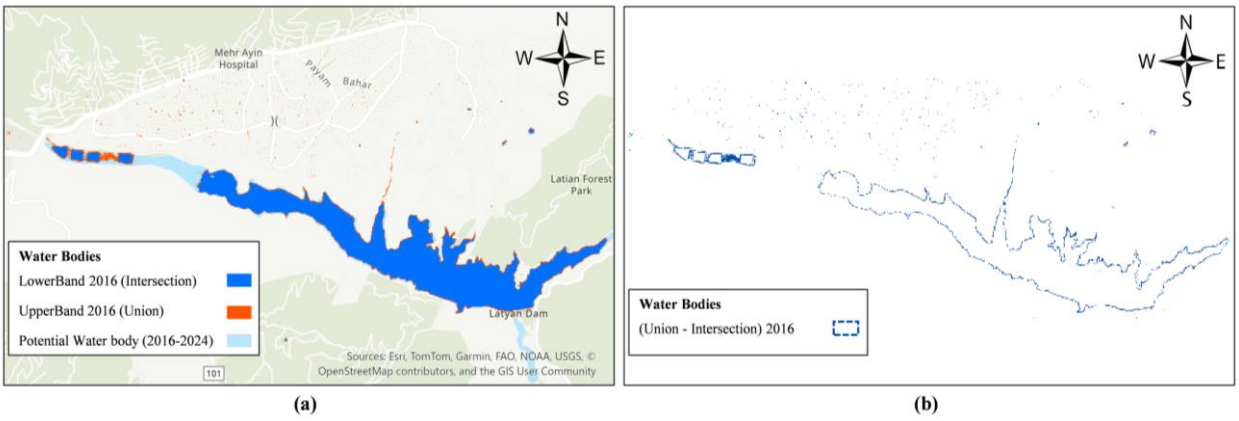

Fig. 3. 2016 Water area for a: union and intersection of implemented indices, b: union-intersection

The time series analysis of water body extents, as shown in Fig. 4, highlights the changes in areas calculated by NDWI, MNDWI, and AWEIsh indices, along with their union (OR) and intersection (AND). The highest extent was observed in 2016, with a value of approximately 3.3 km², while the lowest extent occurred in 2023, measuring about 1.1 km². Trendlines for the union and intersection indicate a decreasing trend from 2016 to 2024, suggesting a consistent reduction in water body extent over the study period. This significant decline warrants further investigation, which could be attributed to anthropogenic activities such as excessive river water extraction for agricultural, industrial, or domestic purposes, as well as climatic factors like drought and dry years affecting the region.

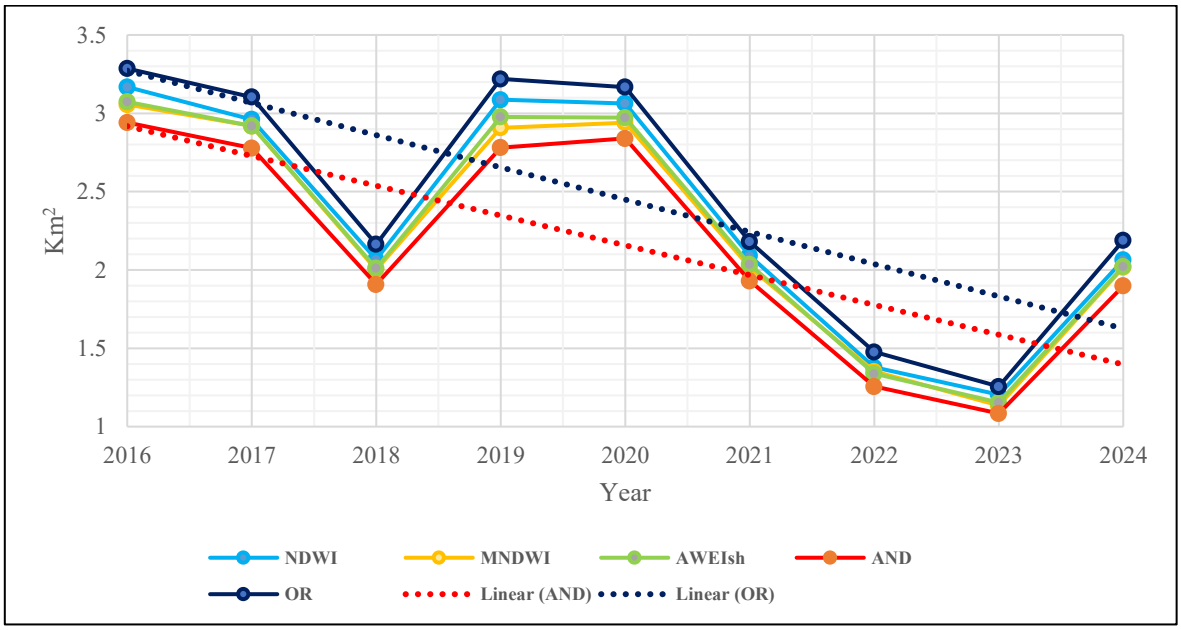

Fig. 4. Covered area of the calculated indices, union and intersection

Figures 5a and 5b further illustrate the calculated extents of NDWI, MNDWI, and AWEIsh indices for the wettest year (2016) and driest year (2023), respectively. These figures reveal minimal differences in water body detection among the three indices,

demonstrating their comparable performance in delineating water extent despite significant changes in climatic conditions between the two years.

The value of each cell in the final water area picture for different indices is between -1 to 1, where values greater than 0 are assumed as water surface. The mean value of the water extent for each index yearly is provided in Fig. 5. The observed differences in the mean values of cells greater than 0 across the indices can be attributed to their varying sensitivities to environmental features and their specific methodologies for water detection. NDWI, MNDWI, and AWEIsh each prioritize different spectral characteristics, leading to discrepancies in water surface delineation, particularly in marginal or mixed pixels. Additionally, the union of all three indices likely includes pixels from non-water areas, such as urban features within the city located to the north of the reservoir, which act as outliers and inflate the final calculated water extent. To improve accuracy, a more restrictive approach that focuses on the lower band of water body detection should be adopted, ensuring the exclusion of urban and non-relevant pixels. This refined methodology would yield a more precise representation of the water surface area behind the reservoir.

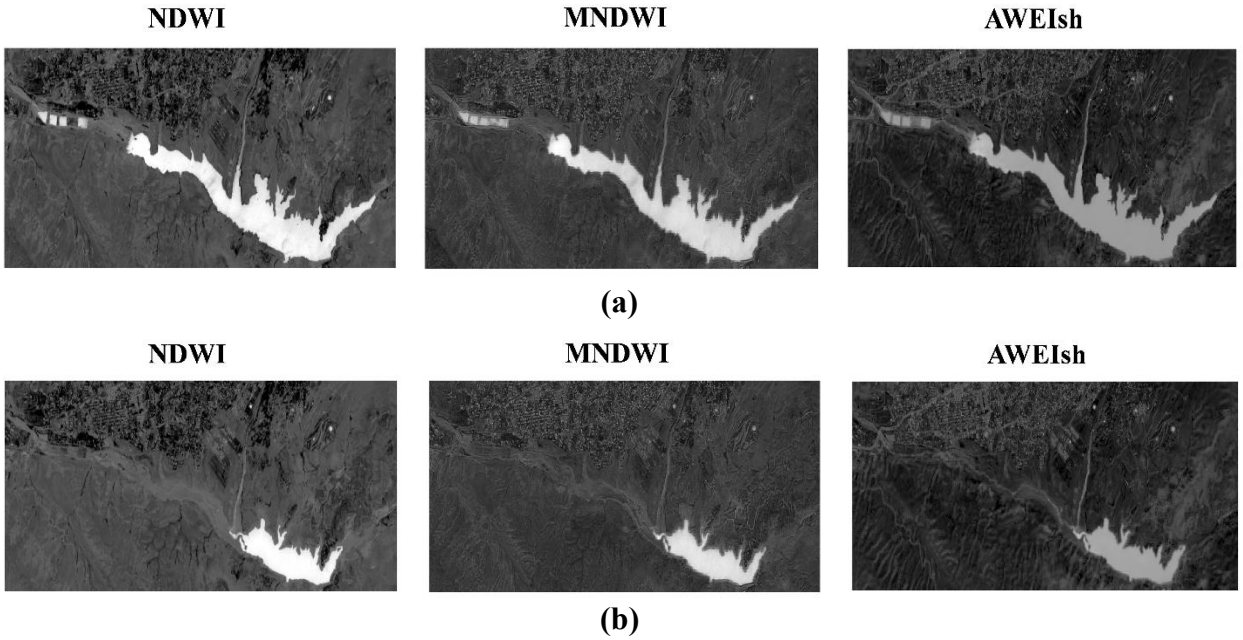

Fig. 5. The final water area extracted from different indices for the driest and wettest years: a: 2016 and b: 2023.

Figure 6 illustrates the temporal variations in the water extent of the Latyan Dam Reservoir using three water indices: NDWI, MNDWI, and AWEIsh. The vertical axis represents different years, showing the interannual changes in the reservoir's surface water coverage. The horizontal axis differentiates the results obtained from the three indices, allowing for a comparative evaluation of their performance in delineating the water body.

Figure 7 presents the areas of uncertainty in water extent detection for the Latyan Dam Reservoir from 2016 to 2024, derived by subtracting the intersection of the indices from their union. The highlighted regions represent the difference between the union and intersection of water surfaces detected by the three indices (NDWI, MNDWI, and AWEIsh). These areas indicate pixels where at least one index classified them as water, but not all three, suggesting potential misclassification or sensitivity differences among the indices

A comparison was conducted with the study of Sorkhabi et al. (2022), who evaluated the water storage variations of the Latyan Dam Reservoir using remote sensing data and artificial intelligence techniques. Although their research focused on reservoir water storage (km^3) and the present study estimates water surface extent (km^2), both investigations reveal a consistent decreasing trend over the study period, indicating an overall decline in reservoir conditions. Both studies identified

2016 as the wettest year. In Sorkhabi et al. (2022), the maximum storage volume was reported as 2.94 km³, while in the present study, the maximum water surface area was estimated at 3.3 km².

Regarding dry conditions, their results indicated that 2022 was the driest year within their study period, with a minimum storage of 1.1 km³. Correspondingly, our surface area analysis showed a marked reduction in 2022 (1.5 km²), identifying it as the second driest year. However, because their study period concluded in 2022, subsequent years were not evaluated. By extending the analysis through 2024, the present study identified 2023 as the driest year, with a minimum water surface area of 1.3 km². Despite differences in hydrological indicators (storage volume versus surface extent), the findings of both studies are consistent in identifying wet and dry extremes and confirming the overall declining pattern of the reservoir.

3.1.Reflectance Distribution

The blue histograms in Fig. 8 illustrate the pixel reflectance distribution for the three indices (NDWI, MNDWI, and AWEIsh) during the wettest year (2016) and the driest year (2023). NDWI exhibits higher peaks in 2016 compared to 2023, reflecting a more extensive water presence across the study area. Similarly, MNDWI follows the same trend, with a broader histogram in 2016, signifying larger water-covered regions. In contrast, in 2023, the NDWI and MNDWI values are significantly lower, indicating a reduction in water extent. The narrowing of histograms for 2023 suggests that water pixels are more constrained, with limited spatial coverage. Additionally, AWEIsh values in 2016 demonstrate a better spread, showing that shadows had a lesser impact that year, whereas in 2023, they become more constrained, reflecting reduced water-covered areas.

Fig. 6. Temporal and index-based variation of latyan dam reservoir water extent (from left to right NDWI, MNDWI, AWEIsh) from 2016 (at the top) until 2024 (at the bottom)

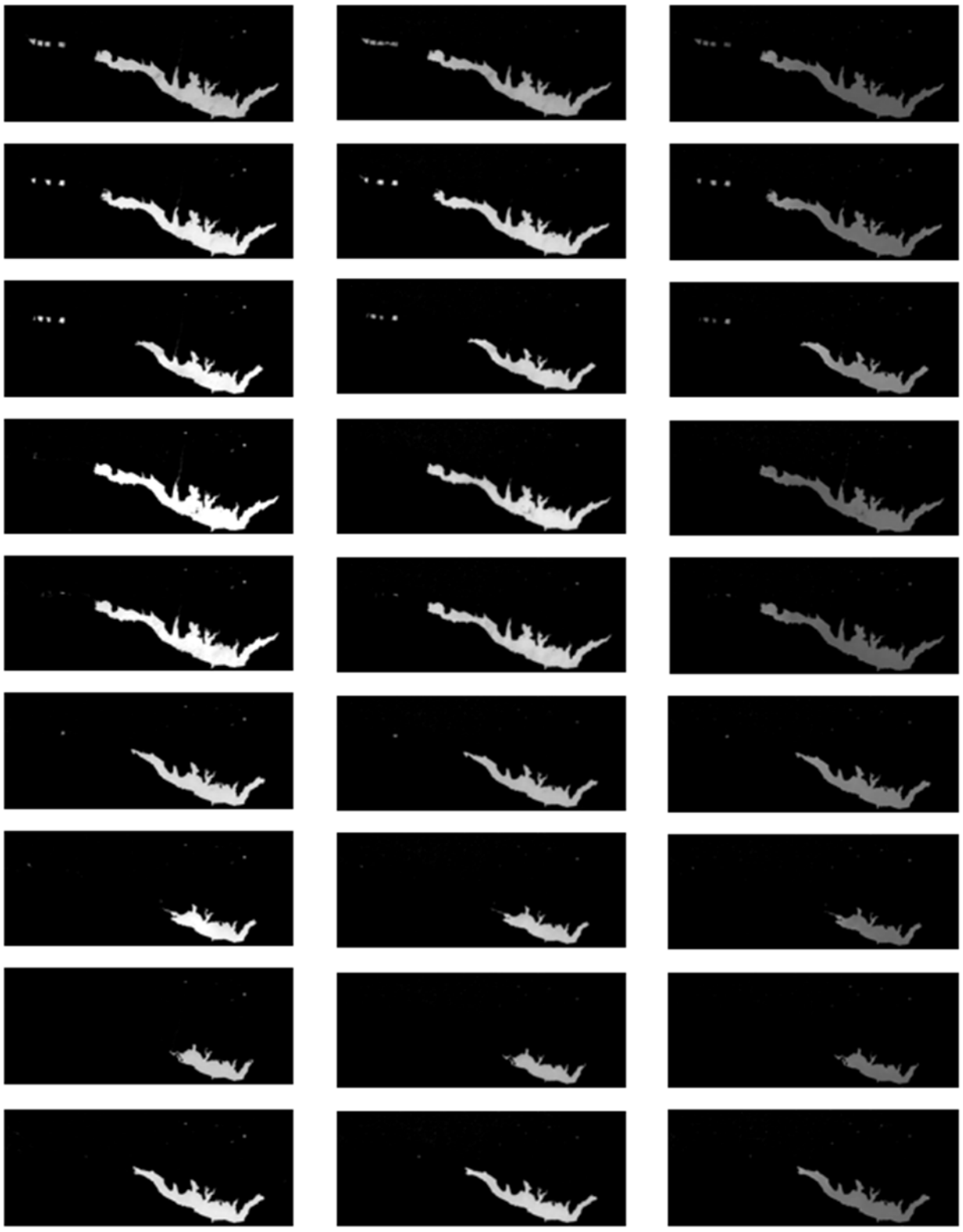

Fig. 7. Uncertainty in water extent detection across indices

The cumulative distribution functions (red graphs) provide further insights into water extent differences between 2016 and 2023. In 2016, the cumulative distributions rise more gradually, indicating an even spread of reflectance values across the study area. This suggests a more continuous and well-defined water body, with smoother transitions between land and water. However, in 2023, the cumulative curves exhibit a much steeper increase and level off earlier, signifying fewer water-covered pixels and sharper boundaries between water and non-water regions. This steep rise in 2023 reflects a more fragmented and constrained water presence, with fewer areas contributing to the cumulative distribution.

3.2. Comparison Between AND and OR Classifications

The comparison between the AND (intersection of indices) and OR (union of indices) classifications highlights differences in water detection stability. In 2016, the AND distribution shows a strong concentration of higher values, suggesting strong agreement among NDWI, MNDWI, and AWEIsh in identifying water-covered areas. However, in 2023, the distribution is much narrower, indicating less agreement between indices and a reduced water-covered area. On the other hand, the OR distribution in 2016 captures a wider range of values, likely incorporating transitional zones between land and water. In contrast, in 2023, the OR distribution is significantly narrower, further confirming the decline in water coverage. The sharper cutoff in the cumulative curve for 2023 underscores the overall reduction in water extent, as fewer pixels meet the water classification criteria.

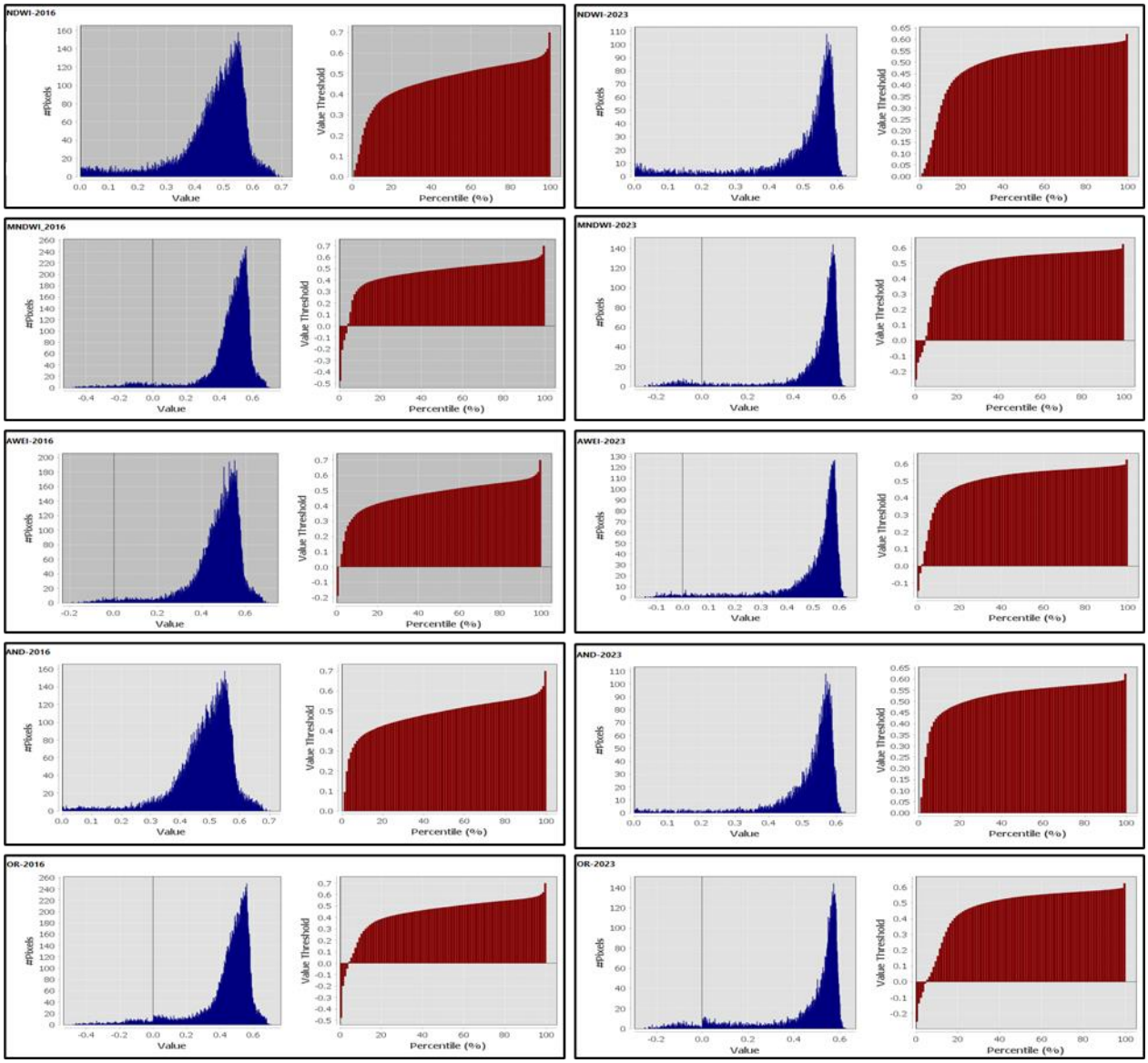

Fig. 8. Computed statistics for NDWI, MNDWI, AWEIsh, lower band and upper band for the wettest year (2016, left section) and the driest year (2023, right section)

3.3. Comparison of Fixed and Adaptive Thresholding

To evaluate the robustness of the fixed threshold (index ≥ 0) used for water classification, an adaptive thresholding approach based on the Otsu method was also applied. The comparison was conducted for two representative hydrological conditions: the wettest year (2016) and the driest year (2023). These years were selected to capture contrasting optical and climatic conditions, thereby enabling assessment of threshold stability under extreme scenarios. For each spectral index (NDWI, MNDWI, and

AWEIsh), image-specific thresholds were derived using the Otsu algorithm, and corresponding water pixels, water percentages, and uncertainty bands (defined by the difference between union and intersection classifications) were calculated. The results for both thresholding approaches are summarized in Table 2.

Table 2. Calculated thresholds, pixels & water percentage of Fixed value & Otsu method

Year	Indices	Otsu			Fixed Value		
		Threshold	Water Pixels	Water Percentage	Threshold	Water Pixels	Water Percentage
2016	NDWI	0.087	30867	8.85	0	31660	9.07
	MNDWI	-0.0011	30574	8.76	0	30540	8.75
	AWEIsh	-0.1733	37350	10.71	0	30711	8.8
	AND	0.002	29126	8.33	0	29394	8.43
	OR	0.002	37376	10.71	0	32840	9.41
2023	NDWI	0.1117	11486	3.29	0	12032	3.45
	MNDWI	0.009	11228	3.22	0	11344	3.25
	AWEIsh	-0.1836	17815	5.11	0	11538	3.31
	AND	0.002	10638	3.05	0	10838	3.11
	OR	0.002	17829	5.11	0	12556	3.6

The comparison indicates that, for NDWI and MNDWI, the Otsu-derived thresholds are consistently close to zero in both years, suggesting that the commonly used fixed threshold aligns well with data-driven separation of water and non-water pixels. While the Otsu method produced more variable thresholds for AWEIsh, this resulted in larger differences between union and intersection classifications, reflecting increased sensitivity to marginal or mixed pixels.

Importantly, the application of adaptive thresholding did not alter the identification of wettest and driest years, nor did it affect the overall temporal trend of decreasing water extent. In contrast, the fixed threshold approach yielded more stable classification results and narrower uncertainty bands, particularly when combined with the intersection method. These findings support the use of a fixed threshold (index ≥ 0) as a robust and consistent criterion for long-term reservoir water extent monitoring in this study.

3.4. Limitations

While the multi-index framework and uncertainty quantification adopted in this study provide a consistent basis for inter-annual surface water monitoring, several limitations should be acknowledged. The absence of in-situ observations, high-resolution reference imagery, and an official stage–storage (elevation–volume) relationship prevented external quantitative validation of absolute surface area estimates and restricted the derivation of reservoir storage volume. Furthermore, although uncertainty zones were qualitatively associated with shoreline transition areas and mixed pixels, a fully systematic attribution of discrepancies to specific scene characteristics (e.g., vegetation, shadow, or urban adjacency) was constrained by the lack of auxiliary ground or higher-resolution data. Future integration of field measurements, bathymetric surveys, or independent validation datasets would further strengthen the quantitative robustness and operational applicability of the results.

4. Conclusion

This study demonstrates the effectiveness of Sentinel-2 imagery and water indices in monitoring reservoir surface area variations, with a specific focus on the Latyan Dam. The integration of NDWI, MNDWI, and AWEIsh indices, along with their intersection and union methods, improves the accuracy of water body delineation. The results reveal significant fluctuations in water extent, which can be attributed to seasonal variations, climate change, and human activities such as water extraction and land use changes. By utilizing freely available satellite data and an automated

workflow in SNAP, this approach offers a scalable and efficient method for monitoring reservoirs in data-scarce regions.

The multi-index analysis of NDWI, MNDWI, and AWEIsh revealed a persistent decline in the Latyan Reservoir's surface water extent between 2016 and 2024, with the maximum area of 3.3 km² in 2016 and a minimum of 1.1 km² in 2023. The difference between the union (OR) and intersection (AND) classifications, interpreted as an uncertainty band, remained relatively small and generally ranged from about 0.2 to 0.4 km², with slightly reduced values in dry years, indicating that most pixels were consistently classified across indices. Reflectance distributions confirmed broader, higher positive values in 2016 and narrower, lower responses in 2023, consistent with the observed shrinkage in water surface area. Comparison of thresholding strategies showed that the fixed global threshold (index ≥ 0) produced more stable and conservative water masks than Otsu thresholding, reducing uncertain pixels from 8250 to 3446 in 2016 and from 7191 to 1718 in 2023. These results suggest that combining a global threshold with multi-index intersection is a robust approach for long-term reservoir monitoring and aligns with independent evidence of declining storage in the Latyan system.

Although the present study focused on monitoring reservoir surface area, estimation of storage volume from remotely sensed data is feasible when an elevation–surface–storage (stage–storage) relationship is available. In addition, empirical surface–volume relationships have been successfully developed using remote sensing combined with field measurements (e.g., Hameed et al., 2022; Phankamolsil & Kositsakulchai, 2020) and through power-law formulations relating area to storage (Francis et al., 2020; Tunji et al., 2020). Therefore, integrating stage–storage data or calibrated empirical models could represent a valuable extension of this research in future studies to enhance its practical and operational applicability.

Additionally, the observed trends in water availability contribute to drought monitoring efforts and help assess the long-term impacts of climate change on regional hydrology. Furthermore, distinguishing between natural and anthropogenic influences on water body fluctuations aids in policy-making and sustainable water allocation. Future research could enhance this approach by integrating additional remote sensing datasets, incorporating machine learning techniques, or validating results with in-situ measurements to improve precision and reliability.

5. Conflict of interests

No potential conflict of interest was reported by the authors.

6. References

Alahacoon, N., & Edirisinghe, M. (2022). A comprehensive assessment of remote sensing and traditional based drought monitoring indices at global and regional scale. Geomatics, *Natural Hazards and Risk, 13*(1), 762–799. https://doi.org/10.1080/19475705.2022.2044394.

Assiri, M. E., Ali, M. A., Siddiqui, M. H., AlZahrani, A., Alamri, L., Alqahtani, A. M., & Ghulam, A. S. (2024). Remote Sensing Assessment of Water Resources, Vegetation, and Land Surface Temperature in Eastern Saudi Arabia: Identification, Variability, and Trends. *Remote Sensing Applications: Society and Environment, 36*, 101296. https://doi.org/10.1016/j.rsase.2024.101296.

Chen, C., Qin, Q., Chen, L., Zheng, H., Fa, W., Ghulam, A., & Zhang, C. (2015). Photometric correction and reflectance calculation for lunar images from the Chang'E-1 CCD stereo camera. Journal of the Optical Society of America A, 32(12), 2409-2422. https://doi.org/10.1364/JOSAA.32.002409.

Drusch, M., Del Bello, U., Carlier, S., Colin, O., Fernandez, V., Gascon, F., ... & Bargellini, P. (2012). Sentinel-2: ESA's optical high-resolution mission for GMES operational services. *Remote Sensing of Environment, 120*, 25–36. https://doi.org/10.1016/j.rse.2011.11.026.

Du, Y., Zhang, Y., Ling, F., Wang, Q., Li, W., & Li, X. (2016). Water bodies' mapping from Sentinel-2 imagery with modified normalized difference water index at 10-m spatial resolution produced by sharpening the SWIR band. *Remote Sensing, 8*(4), 354. https://doi.org/10.3390/rs8040354.

Feyisa, G. L., Meilby, H., Fensholt, R., & Proud, S. R. (2014). Automated Water Extraction Index: A new technique for surface water mapping using Landsat imagery. *Remote Sensing of Environment, 140*, 23–35. https://doi.org/10.1016/j.rse.2013.08.029.

Francis, O. I., Anornu, G. K., Adjei, K. A., & Martin, E. O. (2021). Development of water surface area–storage capacity relationship using empirical model for Gurara reservoir, Nigeria. *Modeling Earth Systems and Environment, 7*(3),

2047-2058. https://doi.org/10.1007/s40808-020-00949-w.

Gu, Z., Zhang, Y., & Fan, H. (2021). Mapping inter-and intra-annual dynamics in water surface area of the Tonle Sap Lake with Landsat time-series and water level data. *Journal of Hydrology, 601*, 126644. https://doi.org/10.1016/j.jhydrol.2021.126644.

Hameed, F., Qureshi, M. A., & Khalil, R. M. Z. (2022). Establishing level-area-volume relationships of Darawat reservoir using time series remote-sensing images. https://doi.org/10.21203/rs.3.rs-1237194/v1.

Koto, A. G., Syahrial, S., & Asruddin, A. (2026, January). The use of water index transformation for surface water detection based on google earth engine. In *AIP Conference Proceedings* (Vol. 3337, No. 1, p. 030019). AIP Publishing LLC. https://doi.org/10.1063/5.0296477.

Liu, H., Hu, H., Liu, X., Jiang, H., Liu, W., & Yin, X. (2022). A comparison of different water indices and band downscaling methods for water bodies mapping from Sentinel-2 imagery at 10-M resolution. *Water, 14*(17), 2696. https://doi.org/10.3390/w14172696.

McFeeters, S. K. (1996). The use of the Normalized Difference Water Index (NDWI) in the delineation of open water features. *International Journal of Remote Sensing, 17*(7), 1425–1432. https://doi.org/10.1080/01431169608948714.

Melkamu, T., Bagyaraja, M., & Adimaw, M. (2022). Spatiotemporal change assessment of Lake Beseka, Ethiopia using time series Landsat images. *Hydrospatial Analysis*, *6*(1), 27-39. https://doi.org/10.21523/gcj3.2022060103.

Mizuochi, H., Hiyama, T., Ohta, T., & Nasahara, K. N. (2014). Evaluation of the surface water distribution in north-central Namibia based on MODIS and AMSR series. *Remote Sensing*, *6*(8), 7660-7682. https://doi.org/10.3390/rs6087660.

Özelkan, E. (2020). Water body detection analysis using NDWI indices derived from landsat-8 OLI. *Polish Journal of Environmental Studies, 29*(2), 1759-1769. https://doi.org/10.15244/pjoes/110447.

Phankamolsil, Y., & Kositsakulchai, E. (2020). Revision of Vajiralongkorn Dam's reservoir characteristic curves using NDWI derived from Landsat 8 Data. *Environment and Natural Resources Journal, 18*(2), 134-145. https://doi.org/10.32526/ennrj.18.2.2020.13.

Rokni, K., Ahmad, A., Selamat, A., & Hazini, S. (2014). Water feature extraction and change detection using multitemporal Landsat imagery. *Remote sensing*, *6*(5), 4173-4189. https://doi.org/10.3390/rs6054173.

Sekertekin, A. (2021). A survey on global thresholding methods for mapping open water body using Sentinel-2 satellite imagery and normalized difference water index. *Archives of Computational Methods in Engineering, 28*(3), 1335–1347. https://doi.org/10.1007/s11831-020-09416-2.

Sharma, R. C., Tateishi, R., Hara, K., & Nguyen, L. V. (2015). Developing superfine water index (SWI) for global water cover mapping using MODIS data. *Remote Sensing, 7*(10), 13807–13841. https://doi.org/10.3390/rs71013807.

Sorkhabi, O. M., Shadmanfar, B., & Kiani, E. (2022). Monitoring of dam reservoir storage with multiple satellite sensors and artificial intelligence. *Results in Engineering, 16*, 100542. https://doi.org/10.1016/j.rineng.2022.100542.

Ticehurst, C., Teng, J., & Sengupta, A. (2022). Development of a multi-index method based on Landsat reflectance data to map open water in a complex environment. *Remote Sensing, 14*(5), 1158. https://doi.org/10.3390/rs14051158.

Tunji, L. A. Q., Sempewo, J. I., & Mbatya, W. (2020). Development of a water surface area-storage capacity relationship for Namodope Reservoir, Uganda. *Journal of Applied Water Engineering and Research, 8*(3), 183-193. https://doi.org/10.1080/23249676.2020.1787243.

Varghese, D., Radulović, M., Stojković, S., & Crnojević, V. (2021). Reviewing the potential of Sentinel-2 in assessing the drought. *Remote Sensing, 13*(17), 3355. https://doi.org/10.3390/rs13173355.

Wang, X., Xie, S., Zhang, X., Chen, C., Guo, H., Du, J., & Duan, Z. (2018). A robust Multi-Band Water Index (MBWI) for automated extraction of surface water from Landsat 8 OLI imagery. *International Journal of Applied Earth Observation and Geoinformation, 68*, 73–91. https://doi.org/10.1016/j.jag.2018.01.018.